Wang *et al. Energy Mater* 2024;4:400032
DOI: 10.20517/energymater.2023.123

Energy Materials

Article

Open Access

Check for updates

Single-atomic-Ni electrocatalyst derived from phthalocyanine-modified MOF for convoying CO_2 intelligent utilization

San-Mei Wang[1,2,5], Xiaoshi Yuan[1,2,5], Shenghua Zhou[2], Xiaofang Li[2], Shu-Guo Han[2], Wenlie Lin[2], Lirong Zheng[4], Dong-Dong Ma[2,*], Qi-Long Zhu[2,3,*]

[1]College of Chemistry, Fuzhou University, Fuzhou 350002, Fujian, China.
[2]State Key Laboratory of Structural Chemistry, Fujian Institute of Research on the Structure of Matter, Chinese Academy of Sciences (CAS), Fuzhou 350002, Fujian, China.
[3]School of Materials Science and Engineering, Zhejiang Sci-Tech University, Hangzhou 310018, Zhejiang, China.
[4]Beijing Synchrotron Radiation Facility, Institute of High Energy Physics, Chinese Academy of Sciences, Beijing 100049, China.
[5]Fujian College, University of Chinese Academy of Sciences, Fuzhou 350002, Fujian, China.

***Correspondence to:** Prof. Dong-Dong Ma, State Key Laboratory of Structural Chemistry, Fujian Institute of Research on the Structure of Matter, Chinese Academy of Sciences (CAS), 155 Yangqiao Road West, Gulou District, Fuzhou 350002, Fujian, China. E-mail: madong@fjirsm.ac.cn; Prof. Qi-Long Zhu, State Key Laboratory of Structural Chemistry, Fujian Institute of Research on the Structure of Matter, Chinese Academy of Sciences (CAS), 155 Yangqiao Road West, Gulou District, Fuzhou 350002, Fujian, China. E-mail:qlzhu@fjirsm.ac.cn

How to cite this article: Wang SM, Yuan X, Zhou S, Li X, Han SG, Lin W, Zheng L, Ma DD, Zhu QL. Single-atomic-Ni electrocatalyst derived from phthalocyanine-modified MOF for convoying CO_2 intelligent utilization. *Energy Mater* 2024;4:400032. https://dx.doi.org/10.20517/energymater.2023.123

Received: 28 Dec 2023 **First Decision:** 26 Feb 2024 **Revised:** 9 Mar 2024 **Accepted:** 26 Mar 2024 **Published:** 9 Apr 2024

Academic Editor: Huajie Yin, Hong Xu **Copy Editor:** Fangyuan Liu **Production Editor:** Fangyuan Liu

Abstract

Single-atomic-site catalysts have been demonstrated as promising candidates for electrochemical CO_2 reduction reaction (eCO_2RR). However, the universal construction strategies need to be further developed to synthesize the desired single-atomic-site catalysts with high eCO_2RR activity for feasible CO_2 utilization. Herein, a novel 2-methylimidazole-phthalocyanine-Ni (IM_4NiPc) coordinatively modified ZIF-8 was rationally fabricated and applied to derive the single-atomic-Ni electrocatalyst (Ni-N-C-I), which is capable of delivering much improved activity for eCO_2RR, compared to the pristine IM_4NiPc immobilized onto ZIF-8-derived N-doped carbon surface, and is also comparable to the best reported catalysts. The satisfied Faradaic efficiency, current density and stability of CO_2-to-CO electroconversion over Ni-N-C-I are shown to originate from the verified Ni-N_4 configuration, particularly, reaching a CO Faradaic efficiency of 99% in a wide potential range. Moreover, based on the outstanding eCO_2RR activity of Ni-N-C-I, we successfully realized the exemplary synthesis of amide polymer materials through CO-

mediated electro/thermocatalytic cascade processes, demonstrating the feasibility of utilizing CO_2 for material manufacturing. This finding is expected to provide useful insight on the precise design and rational synthesis of the novel single-atomic-site catalysts for future CO_2 intelligent utilization.

Keywords: Single-atomic-site catalysts, electrochemical CO_2 reduction reaction, electro/thermocatalytic cascade process, amide polymers

INTRODUCTION

A strategy that kills three birds with one stone has attracted extensive attention, that is, electrocatalytic CO_2 reduction systems, which not only convert excess CO_2 to alleviate environmental issues but also generate value-added industrial feedstocks and especially store the intermittent renewable energy[1-5]. Although electrocatalytic CO_2 reduction reaction (eCO_2RR) can be operated under mild conditions, it still faces some problems such as efficient activation of CO_2 to confront competitive hydrogen evolution reaction, economic construction of electrocatalysts and upgrading separation of products to optimize costs and benefits[6-10]. Currently, in order to overcome these bottlenecks, by screening various electrocatalytic materials and understanding their structure-activity relationships in eCO_2RR, it is imperative to further develop effective, economical, and environmentally friendly strategies for constructing new electrocatalysts.

In virtue of structural and visual identification guided by X-ray absorption spectroscopy, aberration-corrected high-angle annular dark-field scanning transmission electron microscopy, and other techniques, the single-atomic-site catalysts featuring high selectivity, efficient atom utilization, well-defined catalytic site, *etc.*, have exponentially grown to drive the flourishment of various reactions (e.g., eCO_2RR)[11-20]. Numerous studies have demonstrated that pyrolytic transition metal-based single-atomic-site catalysts (such as Fe, Co, Ni, *etc.*) possess obvious advantages in achieving electrochemical CO_2-to-CO conversion under ordinary conditions[21-30]. More importantly, the construction methods of single-atomic-site electrocatalysts not only determine the selectivity and stability of catalytic reactions but also affect economic issues such as preparation cost[31-33]. Notably, owing to the intelligent designability and versatile functionality of the architectures (such as composition, porosity, *etc.*), the metal-organic frameworks (MOFs), particularly zeolite imidazole frameworks (ZIFs), have been utilized as the platforms for packaging, anchoring and dispersing metal precursors to obtain single-atomic-site electrocatalysts for efficient eCO_2RR[34-40]. For example, pioneeringly, Zhao *et al.* reported that Ni-single atoms (SAs)/N-doped carbon (N-C) derived from ZIF-8 can efficiently drive electrochemical CO_2-to-CO conversion with enhanced current densities and Faradaic efficiencies when compared to Ni nanoparticle-based counterpart[41]. Moreover, by confining metal complexes into ZIF-8, pyrolytically derived single-atomic-site electrocatalysts also achieve selective CO_2 electroreduction[42]. These studies undoubtedly provide scientific references for developing CO_2 electroconversion using low-cost ZIF-8 precursors[43]. Nevertheless, directly using low-concentration and unpurified CO from CO_2 electroconversion for subsequent material manufacturing has great industrial feasibility and flexibility, yet there is a dearth of case studies.

In this work, firstly and innovatively, taking ZIF-8 as the classical casting pattern and unique 2-methylimidazole-phthalocyanine-Ni (IM_4NiPc) as an additive ligand, we successfully constructed a novel pyrolytic single-atomic-Ni catalyst (Ni-N-C-l) to evaluate the electrocatalytic activity of CO_2-to-CO transformation, revealing the optimal activity under economical construction. Concretely, the designed Ni-N-C-l electrocatalyst featuring recognized Ni-N_4 coordination structure shows outstanding CO_2-to-CO stability of 20 h with near-uniform Faradaic efficiencies, which surpasses the vast majority of reported eCO_2RR materials. More importantly, based on the excellent eCO_2RR activity of Ni-N-C-l, we further

demonstrated that the cascade synthesis of amide polymer materials can be achieved through the upgrading of aminocarbonylation with instantly generated CO.

EXPERIMENTAL

Synthesis of Ni-N-C-l

Firstly, 2.30 g of 2-methylimidazole and 0.025 g of IM_4NiPc were dissolved in 30 mL of methanol using ultrasound for 5 min, which was subsequently added into 30 mL of methanol containing 1.04 g of $Zn(NO_3)_2{\cdot}6H_2O$ under vigorous stirring. The obtained solution was stirred for another 24 h. The precipitate, namely ZIF-8-(IM_4NiPc), was collected by centrifugation and washed with methanol for several times and dried in vacuum at 70 °C for 12 h.

Secondly, the above ZIF-8-(IM_4NiPc) powder was heat-treated at 1,000 °C for two hours under Ar atmosphere to produce the Ni-N-C-l catalyst.

Synthesis of Ni-N-C-a

First, 0.05 g of N-C derived from ZIF-8 (carbonized at 1,000 °C) was dispersed in 50 mL of methanol via sonication for 30 min. Next, 30 mL of methanol containing 0.025 g of IM_4NiPc was added to the above solution. After being stirred for 24 h, the Ni-N-C-a catalyst was obtained using a similar collection method.

Polymer engineering

Tris(4-iodophenyl) amine (TIA) (62.1 mg, 0.1 mmol), palladium acetate (10 mg), piperazine or 2-methy piperazine (0.15 mmol), and bis(2-diphenylphosphinophenyl)ether (DPEphos, 10 mg) were added in 8 mL of toluene solution. The mixed solution was heated to 80 °C while continuously pumping in the produced gas from eCO_2RR. After reaction for 12 h, the obtained polymer materials were washed with toluene and ethanol and then dried under vacuum at 60 °C.

The additional detailed experimental data, such as reagents, characterizations, and electrochemical measurements, are provided in the supporting information.

RESULTS AND DISCUSSION

Synthesis and characterization of catalysts

Distinguishing traditional introduction of node-evolved or cavity-confined nickel sites, we innovatively designed and synthesized a novel IM_4NiPc molecule with four 2-methylimidazole groups as the additive ligands to introduce the active Ni sites into ZIF-8 (denoted as ZIF-8-(IM_4NiPc), as shown in Supplementary Figure 1 and Figure 1A. Importantly, the feasibility of this strategy is mainly dependent on the IM_4NiPc having good methanolic solubility, well-defined structure [Figure 1B and C][44], and unique coordination ability with Zn^{2+} [Supplementary Figure 2]; other detailed data are shown in the supporting information and Supplementary Figures 3-5. Moreover, Figure 1A further depicts a schematic representation of the synthesis procedure for ZIF-8-(IM_4NiPc) derived Ni-N-C-l catalyst. Meanwhile, for comparison, IM_4NiPc was also immobilized onto congeneric pyrolytic N-C to form the counterpart, labeled as Ni-N-C-a.

Fundamentally, the Ni-N-C-l/a electrocatalysts were controlled to load nearly identical Ni contents to shut out the influence of nickel contents[45,46], as verified by inductively coupled plasma atomic emission spectrometry (ICP-AES) tests [Supplementary Figure 6]. The powder X-ray diffraction (PXRD) patterns in Supplementary Figure 7 and Figure 2A present that ZIF-8-(IM_4NiPc) displays similar characteristic patterns with pristine ZIF-8, indicating the introduction of the IM_4NiPc molecules does not disturb the ZIF-8 framework. Subsequently, the designed two catalysts have been successfully derived from the parent

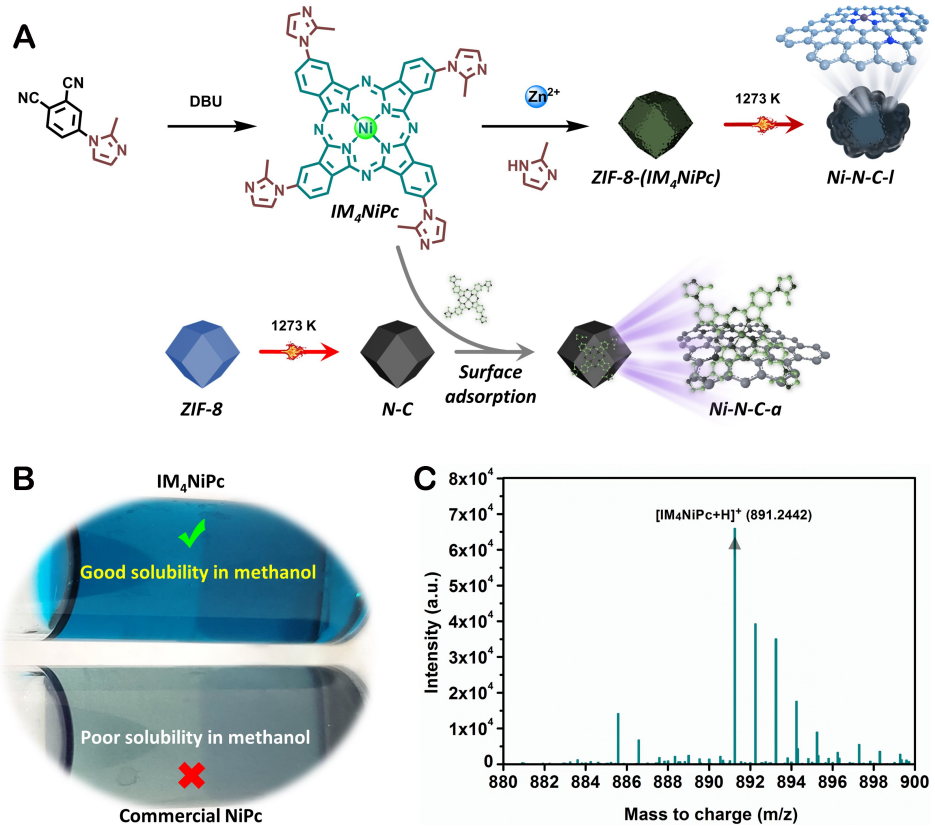

Figure 1. Synthesis illustration of (A) IM_4NiPc, ZIF-8-(IM_4NiPc), Ni-N-C-l and Ni-N-C-a, (B) optical photograph of IM_4NiPc in methanol, and (C) high-resolution mass spectrum of IM_4NiPc.

materials, exhibiting similar carbon characteristics but without any diffraction peaks associated with Ni nanoparticles. This indicates the highly dispersed configuration of Ni species. Furthermore, the Raman spectra of two catalysts reveal low-intensity ratios of the D band to G band [Figure 2B]. Particularly, the designed Ni-N-C-l exhibits a lower ratio value, indicating a higher degree of graphitization due to the participation of IM_4NiPc. It is well-known that pore engineering in catalysts is closely related to the exposure of active sites and continuous mass transfer. Accordingly, representative N_2 sorption isotherms disclose the specific surface areas and pore size distribution of the selected catalysts [Figure 2C and D]. Interestingly, compared to Ni-N-C-a catalyst, the Ni-N-C-l reveals a higher specific surface area of 1,342 $m^2 g^{-1}$, indicating that designing a metallomacrocycle-assisted route is an efficient tactic to construct the accessible single-atom sites. Moreover, the surface compositions and chemical states of the Ni-N-C-l/a were further investigated by X-ray photoelectron spectroscopy (XPS)[47], as depicted in Figure 2E and F. Generally, the N 1s spectra of the selected catalysts can be fitted into five typical peaks corresponding to pyridinic N, metal-N species, pyrrolic N, graphitic N, and oxidized N, respectively[48-50]. Meanwhile, we prudently assigned N species of IM_4NiPc molecules in the N 1s spectrum of the Ni-N-C-a catalyst. In fact, the peak area of graphite N in Ni-N-C-l is larger than that of Ni-N-C-a, which is in agreement with the outcomes of Raman spectra, illustrating the potential higher conductivity of Ni-N-C-l. Impressively, in comparison with Ni^{2+} (855.8 eV) in Ni-N-C-a, the Ni 2p spectrum of pyrolytic Ni-N-C-l indicates the oxidation state of Ni to be between Ni^0 and Ni^{2+}. This finding is in line with previous studies[51-53], further supporting the existence of single Ni atoms.

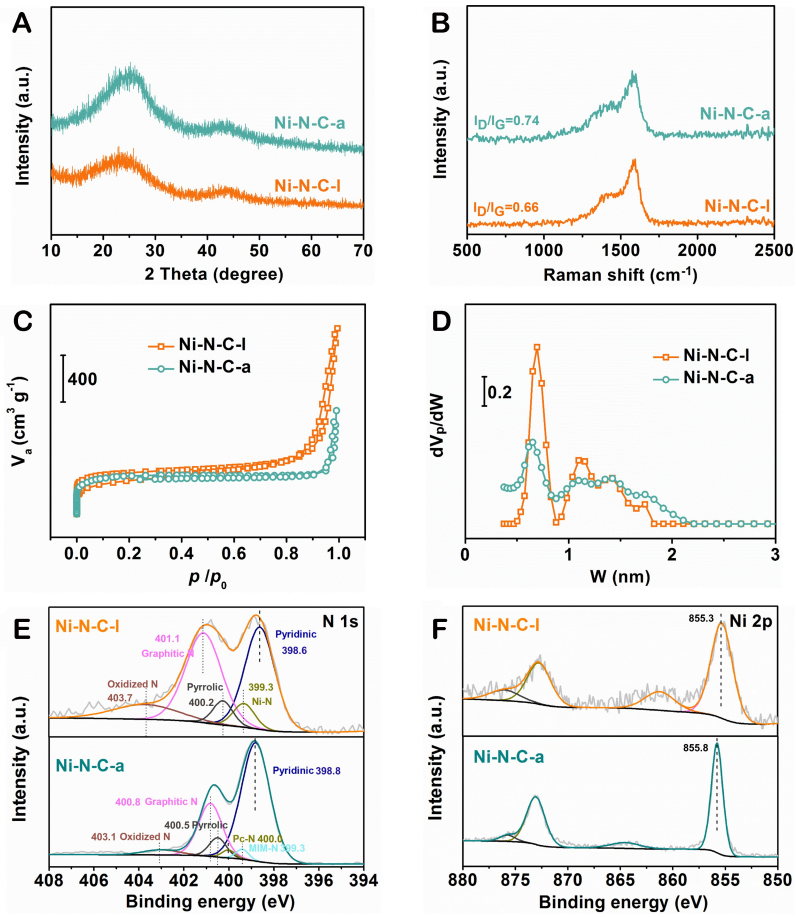

Figure 2. (A) PXRD patterns, (B) Raman spectra, (C) N_2 sorption isotherms, (D) pore size distributions, (E) XPS N 1s and (F) Ni 2p spectra of the designed catalysts.

We next used scanning electron microscopy (SEM) to identify the morphologies of the designed catalysts. Compared with protogenetic ZIF-8, the particle size of ZIF-8-(IM_4NiPc) was significantly reduced after introducing molecular nickel source [Supplementary Figure 8]. After pyrolysis, the Ni-N-C-l material exhibits a shrunk morphology as compared to ZIF-8-(IM_4NiPc) [Supplementary Figure 9]. To further visualize morphologies of the Ni-N-C-l/a, we employed transmission electron microscopy (TEM). As can be observed in Figure 3, Ni-N-C-l displays a fluffed nanoparticle feature consistent with the SEM result, with an absence of metal particles or clusters. Furthermore, the energy-dispersive X-ray (EDX) element mapping images show that Ni, N, and C are uniformly dispersed throughout the sample of Ni-N-C-l [Figure 3B]. This is also observed in the Ni-N-C-a sample [Supplementary Figure 10], which likewise suggests the high dispersity of nickel species at the same scale. More importantly, the aberration-corrected high-angle annular dark-field scanning TEM (AC-HAADF-STEM) image clearly shows that Ni-N-C-l consists of atomically dispersed Ni sites, as evidenced by the distinct white dots in Figure 3C. The X-ray absorption near-edge structure (XANES) spectrum of Ni-N-C-l [Figure 3D], obtained from the Ni K-edge, displays the Ni edge energy of Ni-N-C-l that lies between those of metal foil and NiPc references. This observation suggests that the Ni species in Ni-N-C-l may exist within the valence state of 0 to +2, which agrees with the XPS results. Moreover, the signal of the D_{4h} symmetry structure with 1s to $4p_z$ transition in Ni-N-C-l is lower than that of NiPc, indicating that the symmetric structure of square-planar Ni-N_4 was modulated during pyrolysis. Additionally, the analysis of the Fourier transformed extended X-ray absorption fine structure (EXAFS) supports the existence of atomically dispersed Ni sites with Ni-N

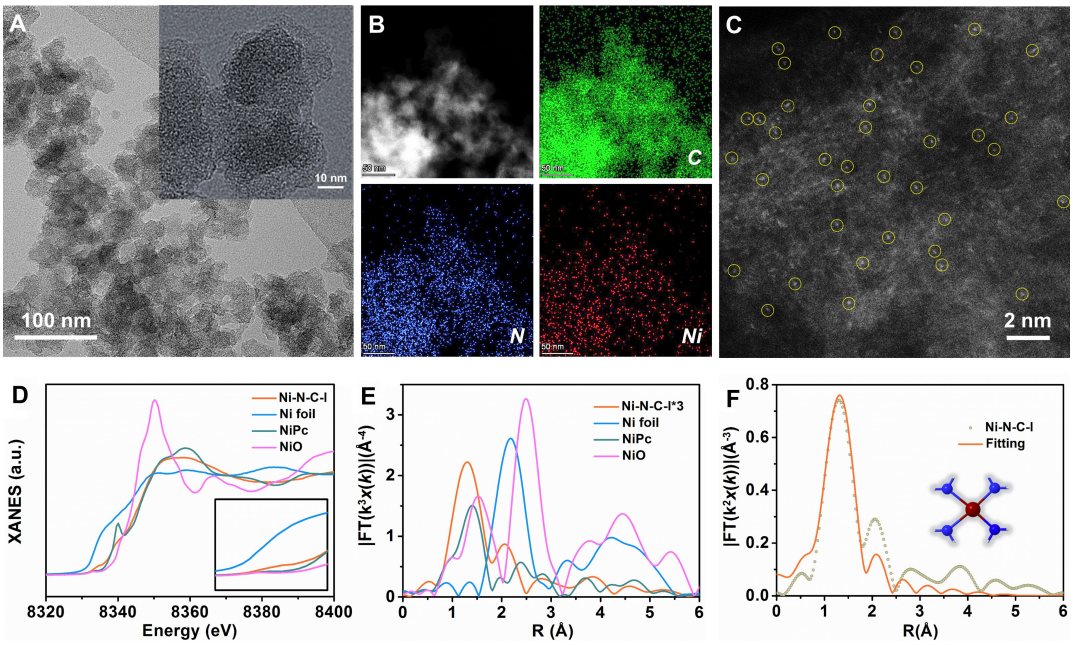

Figure 3. (A) TEM, (B) EDX elemental mapping and (C) AC-HAADF-STEM images of Ni-N-C-l, (D) Ni k-edge XANES and (E) Fourier transformed EXAFS spectra of Ni foil, NiO, NiPc and Ni-N-C-l, (F) EXAFS R-space fitting curve of Ni-N-C-l.

coordination in Ni-N-C-l [Figure 3E], in accordance with the reported works[54-56]. In particular, the fitting analysis is carried out to verify the atomic configuration of Ni-N-C-l; that is, the single Ni atom is coordinated with four N atoms [Figure 3F, Supplementary Figure 11 and Supplementary Table 1].

eCO_2RR performance

Based on the analysis of structures and morphologies mentioned above, the electrocatalytic activities of CO_2 conversion over the comparable catalysts have been evaluated in a typical H-type cell with CO_2-saturated 0.5 M $KHCO_3$ solution. Linear sweep voltammetry (LSV) curves indicate that Ni-N-C-l exhibits an exceptional current density of nearly 70 mA cm^{-2} at -1.1 V, greatly surpassing that of Ni-N-C-a [Figure 4A]. Intriguingly, the LSV curves in Ar-saturated solutions further indicate the contribution of CO_2 electroconversion to current densities [Supplementary Figure 12]. Generally, the reduction products from electrochemical CO_2 conversion were analyzed by off-line ^1H nuclear magnetic resonance (NMR) spectrometer and online gas chromatograph (GC), respectively. By combining the obtained ^1H NMR and GC spectra of Ni-N-C-l operating at -0.78 V [Supplementary Figures 13 and 14], indeed, the only reduction product of CO_2 electroconversion is CO. As shown in Figure 4B and Supplementary Figures 15 and 16, the Ni-N-C-l catalyst exhibits higher Faradic efficiencies of CO (FE_{CO}) within a wider potential window compared to other counterparts. Concretely, the FE_{CO} and current densities of Ni-N-C-l were optimized by controlling the amount of IM_4NiPc (related to active sites) and the carbonization temperature (related to conductivity). Moreover, as observed in Figure 4C and Supplementary Figure 17, the CO partial current densities (j_{CO}) of Ni-N-C-l are better than those of Ni-N-C-a, reaching a j_{CO} of 57.5 mA cm^{-2} at -0.98 V, which is 4.75 times higher than that of Ni-N-C-a. To further emphasize the superiority of Ni-N-C-l in CO_2 electroreduction, it is evident that it exhibits higher turnover frequency (TOF) values [Figure 4D]. Undeniably, the stability is another essential reference for the practical application of catalysts. Figure 4E demonstrates the exceptional long-time durability of Ni-N-C-l, as both j and FE_{CO} almost remain unchanged for continuous electrolysis of 20 h at -0.78 V. This stands in sharp contrast to the Ni-N-C-a counterpart and reported catalysts [Supplementary Table 2], showcasing the outstanding eCO_2RR performance of structure-endowed Ni-N-C-l from multiple perspectives.

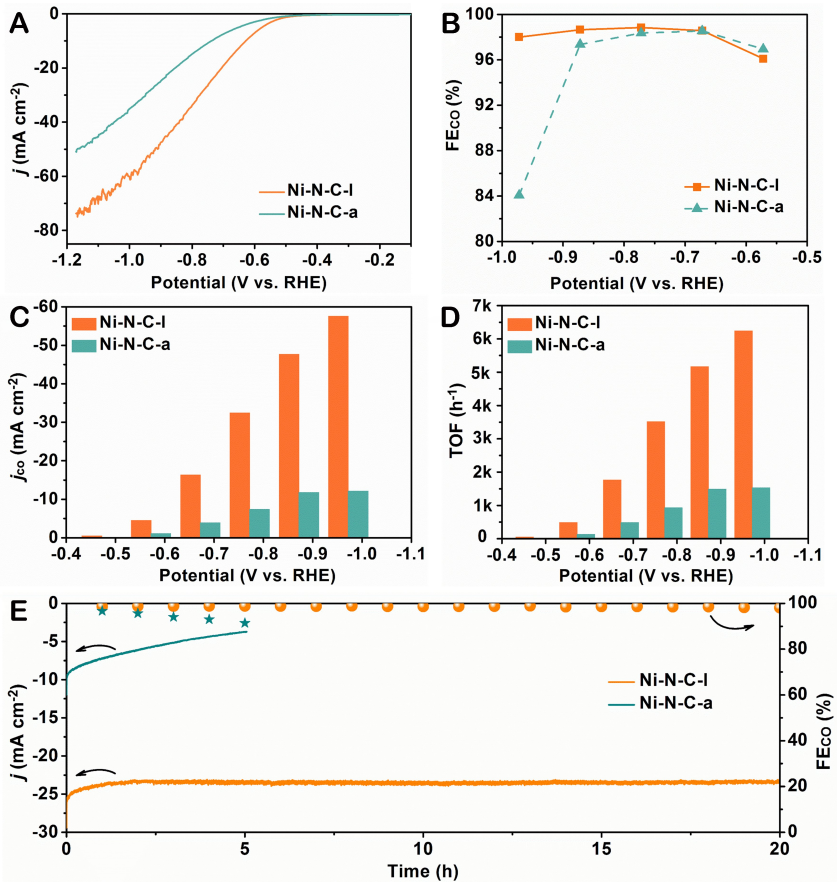

Figure 4. (A) LSV curves, (B) FE_{CO}, (C) j_{CO}, (D) TOFs and (E) long-time durability of Ni-N-C-a and Ni-N-C-l.

To gain a deep understanding of the eCO_2RR kinetics of the investigated catalysts in this system, a fitted Tafel slope of Ni-N-C-l in Supplementary Figure 18 indicates that the first electron transfer to form site-adsorbed intermediates may be the rate-determining step[24,57]. Meanwhile, the electrochemical active areas of the two catalysts were compared by evaluating the electrochemical double-layer capacitances, and the results show that Ni-N-C-l has a larger active surface area [Supplementary Figure 19][58]. In addition, the fast interfacial charge-transfer capacity of Ni-N-C-l during the eCO_2RR is verified by the Nyquist plot in Supplementary Figure 20, as compared to Ni-N-C-a. These findings undeniably demonstrate the inherent high activity of Ni-N-C-l towards CO_2 electroconversion, with a traceable mechanism [Supplementary Figure 21].

Integrated CO_2 electroreduction to polymer engineering

To tackle the issue of economic and efficient product purification, we proposed, for the first time, the direct downstream conversion protocol of CO through polymer engineering. As can be seen in Supplementary Figure 22, we constructed the cascade design by integrating electrocatalysis and thermocatalysis. Interestingly, the two proof-of-concept covalent organic polymers with different functional groups (simplified as COP and COP-Me) were correspondingly obtained by carbonyl insertion under vent gas from CO_2 electroreduction [Figure 5A]. By analyzing XRD patterns and SEM images, we can preliminarily determine the synthesis of amorphous polymers with irregular morphologies [Supplementary Figures 23 and 24]. In order to further confirm the synthesis of target materials, infrared

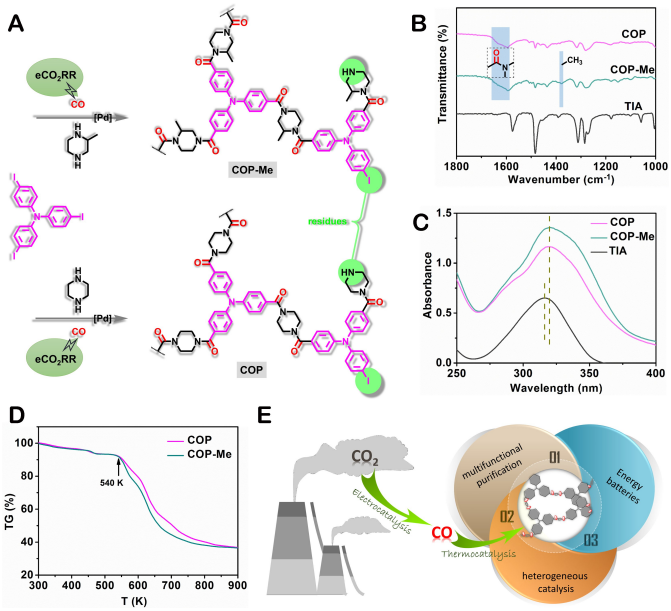

Figure 5. (A) Schematic diagram of designed COP and COP-Me based on CO_2-to-CO steered carbonyl insertion, (B) IR and (C) UV spectra of COP, COP-Me and TIA, (D) TG curves of COP and COP-Me, (E) application diagram of polymer materials from CO_2 conversion.

(IR), ultraviolet (UV) and ^{1}H NMR characterization were performed. As shown in Figure 5B, we can obviously observe the vibration peaks of amide groups at 1,600~1,700 cm^{-1} in the COP and COP-Me, in comparison with tris(4-iodophenyl)amine (TIA). UV-Vis spectra clearly indicate the generation of new skeleton structures with differentiated absorption [Figure 5C]. ^{1}H NMR spectra in Supplementary Figure 25 further reveal the anisotropic C-H environments of polymers compared to the monomer. In addition, thermogravimetric (TG) analysis shows that COP and COP-Me have similar thermal stability [Figure 5D]. In prospect, these industrial CO_2-derived polymer materials may be used in wastewater treatment, precious metal recovery, and other fields [Figure 5E][59,60]. By means of this cascade strategy, the integration of electrochemical CO_2-to-polymer engineering is achieved, meaningfully, offering a potential avenue for future operation.

CONCLUSIONS

In summary, we successfully demonstrated the fabrication of the single-atomic-site catalyst from the phthalocyanine-modified MOF and the novel manufacturing of polymer materials from CO_2 through electro/thermocatalytic cascade processes steered by the designed catalyst. Importantly, the derived Ni-N-C-l catalyst with traceable Ni-N_4 configuration can effectively realize the CO_2-to-CO electroconversion with approximately 100% FE_{CO} and long-term stability, thus guaranteeing the direct intellectual utilization of the unpurified CO generated by eCO_2RR. Particularly, our exotic electro/thermocatalytic cascade system for extending chemical valorization of CO_2 not only highlights the need of the rational design of electrocatalysts but also offers a sustainable and cost-effective strategy for synthesizing valuable amide polymer materials.

DECLARATIONS

Acknowledgments

The authors thank Prof. Xin-Tao Wu for his constructive suggestions.

Authors' contributions

Conceived the research and designed the experiments: Ma DD, Zhu QL
Prepared the phthalocyanines and catalysts: Wang SM
Carried out the electrochemical testing: Wang SM, Yuan X
Carried out the AC-HAADF-STEM measurement: Lin W
Completed the manuscript: Wang SM, Ma DD, Zhu QL
Discussed and revised the manuscript: Wang SM, Yuan X, Zhou S, Li X, Han SG, Lin W, Zheng L, Ma DD, Zhu QL

Availability of data and materials

The details of materials and reagents, instrumentation and characterizations, and electrochemical measurements were shown in the supporting information.

Financial support and sponsorship

The authors are grateful for the financial support of the National Key Research and Development Program of China (2021YFA1500402), the National Natural Science Foundation of China (NSFC) (52332007, 22105203, 22175174, and 22375203), the Natural Science Foundation of Fujian Province of China (2021J06033 and 2022L3092), and the China Postdoctoral Science Foundation (2022M723147).

Conflicts of interest

All authors declared that there are no conflicts of interest.

Ethical approval and consent to participate

Not applicable.

Consent for publication

Not applicable.

REFERENCES

1. Tomboc GM, Choi S, Kwon T, Hwang YJ, Lee K. Potential link between Cu surface and selective CO_2 electroreduction: perspective on future electrocatalyst designs. *Adv Mater* 2020;32:e1908398. DOI
2. Zhu S, Delmo EP, Li T, et al. Recent advances in catalyst structure and composition engineering strategies for regulating CO_2 electrochemical reduction. *Adv Mater* 2021;33:e2005484. DOI
3. Chen S, Li WH, Jiang W, et al. MOF encapsulating N-heterocyclic carbene-ligated copper single-atom site catalyst towards efficient methane electrosynthesis. *Angew Chem Int Ed* 2022;61:e202114450. DOI
4. Ross MB, De Luna P, Li Y, et al. Designing materials for electrochemical carbon dioxide recycling. *Nat Catal* 2019;2:648-58. DOI
5. De Luna P, Hahn C, Higgins D, Jaffer SA, Jaramillo TF, Sargent EH. What would it take for renewably powered electrosynthesis to displace petrochemical processes? *Science* 2019;364:eaav3506. DOI PubMed
6. Khezri B, Fisher AC, Pumera M. CO_2 reduction: the quest for electrocatalytic materials. *J Mater Chem A* 2017;5:8230-46. DOI
7. Lu Q, Rosen J, Zhou Y, et al. A selective and efficient electrocatalyst for carbon dioxide reduction. *Nat Commun* 2014;5:3242. DOI
8. Sa YJ, Lee CW, Lee SY, Na J, Lee U, Hwang YJ. Catalyst-electrolyte interface chemistry for electrochemical CO_2 reduction. *Chem Soc Rev* 2020;49:6632-65. DOI
9. Wang G, Chen J, Ding Y, et al. Electrocatalysis for CO_2 conversion: from fundamentals to value-added products. *Chem Soc Rev* 2021;50:4993-5061. DOI
10. Jia S, Ma X, Sun X, Han B. Electrochemical transformation of CO_2 to value-added chemicals and fuels. *CCS Chem* 2022;4:3213-29. DOI
11. Han SG, Ma DD, Zhu QL. Atomically structural regulations of carbon-based single-atom catalysts for electrochemical CO_2 reduction. *Small Methods* 2021;5:e2100102. DOI PubMed
12. Liu J, Cai Y, Song R, et al. Recent progress on single-atom catalysts for CO_2 electroreduction. *Mater Today* 2021;48:95-114. DOI

13. Wang X, Jia Y, Mao X, et al. Edge-rich Fe-N_4 active sites in defective carbon for oxygen reduction catalysis. *Adv Mater* 2020;32:e2000966. DOI
14. Hu C, Wang Y, Chen J, et al. Main-group metal single-atomic regulators in dual-metal catalysts for enhanced electrochemical CO_2 reduction. *Small* 2022;18:e2201391. DOI
15. Ma D, Han S, Cao C, et al. Bifunctional single-molecular heterojunction enables completely selective CO_2-to-CO conversion integrated with oxidative 3D nano-polymerization. *Energy Environ Sci* 2021;14:1544-52. DOI
16. Su X, Yang XF, Huang Y, Liu B, Zhang T. Single-atom catalysis toward efficient CO_2 conversion to CO and formate products. *ACC Chem Res* 2019;52:656-64. DOI PubMed
17. Li X, Rong H, Zhang J, Wang D, Li Y. Modulating the local coordination environment of single-atom catalysts for enhanced catalytic performance. *Nano Res* 2020;13:1842-55. DOI
18. Zhang E, Wang T, Yu K, et al. Bismuth single atoms resulting from transformation of metal-organic frameworks and their use as electrocatalysts for CO_2 reduction. *J Am Chem Soc* 2019;141:16569-73. DOI
19. Li J, Guan Q, Wu H, et al. Highly active and stable metal single-atom catalysts achieved by strong electronic metal-support interactions. *J Am Chem Soc* 2019;141:14515-9. DOI
20. Wang WL, Santos EJ, Jiang B, et al. Direct observation of a long-lived single-atom catalyst chiseling atomic structures in graphene. *Nano Lett* 2014;14:450-5. DOI
21. Han S, Ma D, Zhou S, et al. Fluorine-tuned single-atom catalysts with dense surface Ni-N_4 sites on ultrathin carbon nanosheets for efficient CO_2 electroreduction. *Appl Catal B Environ* 2021;283:119591. DOI
22. Pan F, Deng W, Justiniano C, Li Y. Identification of champion transition metals centers in metal and nitrogen-codoped carbon catalysts for CO_2 reduction. *Appl Catal B Environ* 2018;226:463-72. DOI
23. Wang C, Ren H, Wang Z, Guan Q, Liu Y, Li W. A promising single-atom Co-N-C catalyst for efficient CO_2 electroreduction and high-current solar conversion of CO_2 to CO. *Appl Catal B Environ* 2022;304:120958. DOI
24. Li Y, Zhang SL, Cheng W, et al. Loading single-Ni atoms on assembled hollow N-rich carbon plates for efficient CO_2 electroreduction. *Adv Mater* 2022;34:e2105204. DOI
25. Yang J, Qiu Z, Zhao C, et al. In situ thermal atomization to convert supported nickel nanoparticles into surface-bound nickel single-atom catalysts. *Angew Chem Int Ed* 2018;57:14095-100. DOI
26. Zhao S, Chen G, Zhou G, et al. A universal seeding strategy to synthesize single atom catalysts on 2D materials for electrocatalytic applications. *Adv Funct Mater* 2020;30:1906157. DOI
27. Li X, Zeng Y, Tung C, et al. Unveiling the in situ generation of a monovalent Fe(I) site in the single-Fe-atom catalyst for electrochemical CO_2 reduction. *ACS Catal* 2021;11:7292-301. DOI
28. Wang C, Liu Y, Ren H, Guan Q, Chou S, Li W. Diminishing the uncoordinated N species in Co-N-C catalysts toward highly efficient electrochemical CO_2 reduction. *ACS Catal* 2022;12:2513-21. DOI
29. Li X, Bi W, Chen M, et al. Exclusive Ni-N_4 sites realize near-unity CO selectivity for electrochemical CO_2 reduction. *J Am Chem Soc* 2017;139:14889-92. DOI
30. Gu J, Hsu CS, Bai L, Chen HM, Hu X. Atomically dispersed Fe^{3+} sites catalyze efficient CO_2 electroreduction to CO. *Science* 2019;364:1091-4. DOI PubMed
31. Li S, Nagarajan AV, Alfonso DR, et al. Boosting CO_2 electrochemical reduction with atomically precise surface modification on gold nanoclusters. *Angew Chem Int Ed* 2021;60:6351-6. DOI
32. He Y, Shi Q, Shan W, et al. Dynamically unveiling metal-nitrogen coordination during thermal activation to design high-efficient atomically dispersed CoN_4 active sites. *Angew Chem Int Ed* 2021;60:9516-26. DOI
33. Liu S, Sun C, Xiao J, Luo J. Unraveling structure sensitivity in CO_2 electroreduction to near-unity CO on silver nanocubes. *ACS Catal* 2020;10:3158-63. DOI
34. Ma D, Zhu Q. MOF-based atomically dispersed metal catalysts: recent progress towards novel atomic configurations and electrocatalytic applications. *Coord Chem Rev* 2020;422:213483. DOI
35. Zhang Y, Jiao L, Yang W, Xie C, Jiang HL. Rational fabrication of low-coordinate single-atom Ni electrocatalysts by MOFs for highly selective CO_2 reduction. *Angew Chem Int Ed* 2021;60:7607-11. DOI
36. Cheng H, Wu X, Feng M, et al. Atomically dispersed Ni/Cu dual sites for boosting the CO_2 reduction reaction. *ACS Catal* 2021;11:12673-81. DOI
37. Yan C, Li H, Ye Y, et al. Coordinatively unsaturated nickel-nitrogen sites towards selective and high-rate CO_2 electroreduction. *Energy Environ Sci* 2018;11:1204-10. DOI
38. Li Y, Adli NM, Shan W, et al. Atomically dispersed single Ni site catalysts for high-efficiency CO_2 electroreduction at industrial-level current densities. *Energy Environ Sci* 2022;15:2108-19. DOI
39. Zeng L, Wang Z, Wang Y, et al. Photoactivation of Cu centers in metal-organic frameworks for selective CO_2 conversion to ethanol. *J Am Chem Soc* 2020;142:75-9. DOI
40. Abdel-Mageed AM, Rungtaweevoranit B, Parlinska-Wojtan M, Pei X, Yaghi OM, Behm RJ. Highly active and stable single-atom Cu catalysts supported by a metal-organic framework. *J Am Chem Soc* 2019;141:5201-10. DOI PubMed
41. Zhao C, Dai X, Yao T, et al. Ionic exchange of metal-organic frameworks to access single nickel sites for efficient electroreduction of CO_2. *J Am Chem Soc* 2017;139:8078-81. DOI
42. Wang Y, Jiang Z, Zhang X, et al. Metal phthalocyanine-derived single-atom catalysts for selective CO_2 electroreduction under high

current densities. *ACS Appl Mater Interfaces* 2020;12:33795-802. DOI

43. Park KS, Ni Z, Côté AP, et al. Exceptional chemical and thermal stability of zeolitic imidazolate frameworks. *Proc Natl Acad Sci USA* 2006;103:10186-91. DOI PubMed PMC
44. Ma D, Han S, Zhou S, et al. Molecularly dispersed heterogenized metallomacrocycles: molecular structure sensitivity of CO_2 electrolysis. *CCS Chem* 2023;5:1827-40. DOI
45. Jiao L, Li X, Wei W, et al. Hierarchically ordered porous superstructure embedded with readily accessible atomic pair sites for enhanced CO_2 electroreduction. *Appl Catal B Environ* 2023;330:122638. DOI
46. Cao C, Zhou S, Zuo S, et al. Si Doping-induced electronic structure regulation of single-atom Fe sites for boosted CO_2 electroreduction at low overpotentials. *Research* 2023;6:0079. DOI PubMed PMC
47. Ma D, Han S, Cao C, Li X, Wu X, Zhu Q. Remarkable electrocatalytic CO_2 reduction with ultrahigh CO/H_2 ratio over single-molecularly immobilized pyrrolidinonyl nickel phthalocyanine. *Appl Catal B Environ* 2020;264:118530. DOI
48. Cheng H, Wu X, Li X, et al. Zeolitic imidazole framework-derived FeN_5-doped carbon as superior CO_2 electrocatalysts. *J Catal* 2021;395:63-9. DOI
49. Zheng T, Jiang K, Ta N, et al. Large-scale and highly selective CO_2 electrocatalytic reduction on nickel single-atom catalyst. *Joule* 2019;3:265-78. DOI
50. Liu C, Wu Y, Sun K, et al. Constructing FeN_4/graphitic nitrogen atomic interface for high-efficiency electrochemical CO_2 reduction over a broad potential window. *Chem* 2021;7:1297-307. DOI
51. Jiao L, Yang W, Wan G, et al. Single-atom electrocatalysts from multivariate metal-organic frameworks for highly selective reduction of CO_2 at low pressures. *Angew Chem Int Ed* 2020;59:20589-95. DOI
52. Petraki F, Papaefthimiou V, Kennou S. The electronic structure of Ni-phthalocyanine/metal interfaces studied by X-ray and ultraviolet photoelectron spectroscopy. *Organic Electronics* 2007;8:522-8. DOI
53. Wang X, Chen Z, Zhao X, et al. Regulation of coordination number over single Co sites: triggering the efficient electroreduction of CO_2. *Angew Chem Int Ed* 2018;57:1944-8. DOI
54. Boppella R, Austeria P M, Kim Y, et al. Pyrrolic N-stabilized monovalent Ni single-atom electrocatalyst for efficient CO_2 reduction: identifying the role of pyrrolic-N and synergistic electrocatalysis. *Adv Funct Mater* 2022;32:2202351. DOI
55. Yang HB, Hung S, Liu S, et al. Atomically dispersed Ni(I) as the active site for electrochemical CO_2 reduction. *Nat Energy* 2018;3:140-7. DOI
56. Jiang K, Siahrostami S, Zheng T, et al. Isolated Ni single atoms in graphene nanosheets for high-performance CO_2 reduction. *Energy Environ Sci* 2018;11:893-903. DOI
57. Geng Z, Cao Y, Chen W, et al. Regulating the coordination environment of Co single atoms for achieving efficient electrocatalytic activity in CO_2 reduction. *Appl Catal B Environ* 2019;240:234-40. DOI
58. Hu M, Wang N, Ma D, Zhu Q. Surveying the electrocatalytic CO_2-to-CO activity of heterogenized metallomacrocycles via accurate clipping at the molecular level. *Nano Res* 2022;15:10070-7. DOI
59. Ou X, Niu Y, Liu Q, et al. Recent progress in CO_2-based polyurethanes and polyureas. *Prog Polym Sci* 2024;149:101780. DOI
60. Zhang N, Wu S, Zheng H, Li G, Liu H, Duan H. Recent progress of multilayer polymer electrolytes for lithium batteries. *Energy Mater* 2023;3:300009. DOI